

Performance Improvement of Liquid Cold Plates for Battery Thermal Management Based On Topology Optimization

Hao Li¹, Huaqiang Liu¹, Tianshuo Yang¹

¹Naval Architecture and Ocean Engineering College, Dalian Maritime University
No. 1 Linghai Rd., Dalian, China

lihao0725@dmlu.edu.cn; huaqiang.liu@dmlu.edu.cn; yts3440926281@dmlu.edu.cn

Abstract - Optimizing the design of cold plate flow paths is essential to augment the efficacy of indirect liquid cooling based battery thermal management systems. This study delves into the impact of varying outlet layouts and initial configurations on the heat transfer capabilities of cold plates based on topology optimization method. The findings reveal that increasing the number of outlets could enhance the heat transfer efficacy of the topologically-optimized cold plates. Specifically, when two outlets were integrated, the heat exchange performance reached its zenith, registering a maximum temperature reduction of 2.48 K (25.7%) and an average temperature decrement of 1.07 K (15.6%) relative to the single-outlet case. Besides, disparate initial structures yield divergent outcomes. Notably, the topology optimization flow channel design based on straight channel exhibited the lowest battery temperature, descending by an additional 0.51 K (7%) compared to its unoptimized counterpart. Concurrently, the uniformly distributed topologically optimized cold plate manifests the least pressure drop, plummeting by 5.22 Pa (30.6%) in contrast to the straight channel cold plate.

Keywords: Lithium-ion batteries, Cold plate, Topology optimization, Outlet layout, Initial structure

1. Introduction

With the depletion of fossil energy and the increasingly serious environmental pollution problem, traditional fossil fuel vehicles are gradually replaced by new energy vehicles, of which electric vehicles are the mainstream. Lithium-ion batteries are widely used as energy sources for electric vehicles because of their high voltage, large specific energy, small size and low self-discharge rate [1]. During operation, lithium-ion batteries are often exposed to a relatively harsh external environment [2]. Temperature is one of key factors that influence the performance of lithium-ion batteries. Thermal runaway may occur if the operating temperature is excess, which will cause the decomposition and spontaneous combustion of the battery [3]. Studies have shown that the ideal working temperature range of lithium-ion batteries is 20-40 °C, and the maximum temperature difference shall be controlled within 5 °C [4].

Commonly used battery thermal management systems (BTMSs) can be divided into air-based, liquid-based and phase change-based methods [5]. Air cooled BTMS is simple and low-cost. However, the heat exchange efficiency is small, which cannot meet the needs of battery cooling under high power and extreme conditions [6]. The thermal management system using phase change materials (PCM) absorbs heat relying on the latent heat. Phase change materials (PCM) can melt or solidify at a given temperature condition, thus control the temperature change of the battery pack [7]. However, challenges also exist for PCM-based BTMS such as long thermal response time and low heat transfer rate [8]. Liquid cooling system is currently the mainstream battery thermal management methods for commercial vehicles and vessels. According to the contact form, it can be divided into direct contact and indirect contact methods. Direct contact refers to that the batteries are directly immersed into the coolant without interval [9]. For indirect contact form, liquid coolant is circulated within the cold plate, pipe or jacket, which is currently the mainstream way of battery thermal management [10]. With the increase of the battery power, the thermal load borne by the battery thermal management system continue to grow, necessitating the research and development of novel cold plate channel structures to further improve the cooling efficiency.

Topology optimization is a relatively new method to design liquid flow channels. It has the advantage of not relying on the designer's experience and having a broader design space. Through the experimental comparison of cold plates in serpentine channels, H. Li [11] demonstrated that topology optimization can effectively improve heat exchange efficiency and reduce flow loss. To date, the research on the topology optimization of liquid cooling plate mainly focuses on the topology optimization parameters, objective functions, and constraints. Most studies have adopted the single-entry single-exit structure, and few studies have studied the multi-exit design. In addition, most studies have adopted the uniformly

distributed initial structure in the topology optimization, and few studies have studied the impact of initial configurations. Therefore, this paper studies the influence of the number of exits and initial structures on the topology optimization results.

2. Topology optimization design of battery cold plate

2.1. Geometric model

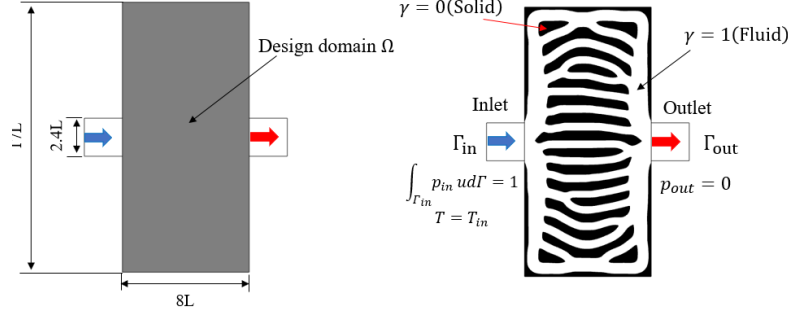


Fig. 1: Topology optimization model: (a) Design domain with dimensions and (b) Boundary conditions.

Because three-dimensional topology optimization would consume massive computational cost and the structures are hard to fabricate, a two-dimensional model was used. The three-dimensional structure is then obtained by extruding the channel topology along the thickness direction. Fig. 1(a) presents the basic dimensions of the initial topology optimization model with uniformly distributed materials. The sizes of the two-dimensional design area are $17L \times 8L$, where L is the characteristic length of the cold plate. The variable density topology optimization method is used. The design variable γ is a pseudo-density parameter that varies continuously between 0 and 1. $\gamma = 1$ means that it is liquid domain, and $\gamma = 0$ manifests the region of solid materials. Constant flow rate and temperature are applied for the inlet, whereas constant pressure of 0 Pa is set for the outlet, and the other boundaries are adiabatic. The integral equation of flow rate and pressure is used to ensure that the input power of the coolant at the inlet of the cold plate is constant.

2.2. Governing equations

The coolant is considered as incompressible viscous fluid, and the governing equations including the continuity equation and momentum conservation equation of the steady-state flow within the cold plate are given as:

$$\nabla \cdot \mathbf{u} = 0 \quad (1)$$

$$\rho(\mathbf{u} \cdot \nabla)\mathbf{u} = -\nabla p + \mu \nabla^2 \mathbf{u} + \mathbf{F} \quad (2)$$

where \mathbf{u} is the velocity vector, p is the pressure, ρ is the density, μ is the viscosity, and \mathbf{F} is the flow resistance.

In the above formula, the volume force \mathbf{F} is the force caused by the fluid flow in the porous medium, and is proportional to the reverse permeability α and the velocity \mathbf{u} . The corresponding calculation formula is as follows:

$$\mathbf{F} = -\alpha \mathbf{u} \quad (3)$$

where α is the inverse permeability of the porous medium and is a function of the design variable γ . The Darcy interpolation model was adopted in this study. Therefore, α can be expressed as:

$$\alpha(\gamma) = \alpha_f + (\alpha_s - \alpha_f) \frac{q(1-\gamma)}{q+\gamma} \quad (4)$$

where α_s and α_f are the reverse permeability of solids and fluids, respectively. In this paper, the value of penalty factor q is 0.01 to avoid being divided by 0. The reverse permeability of fluid α_f is very small, and the value of this paper is 0. The reverse permeability of solid α_s is a large constant, and its value is related to the Reynolds number Re and Darcy number Da . The specific expression is as follows:

$$\alpha_s = \left(1 + \frac{1}{Re}\right) \frac{1}{Da} \quad (5)$$

Dimensionless treatment can reduce the calculation cost and improve the convergence and accuracy of the results. In this paper, the control equation, objective function and restriction conditions in topology optimization calculation are processed without dimension, and the specific calculation formula is shown as follows:

$$\nabla^* = L \nabla \quad Re = \frac{\rho U L}{\mu} \quad \mathbf{u}^* = \frac{\mathbf{u}}{U} \quad p^* = \frac{p}{\rho U^2} \quad (6)$$

where ∇ is the gradient operator, L is the characteristic length, ρ is the fluid density, and U is the characteristic velocity.

Therefore, the dimensionless continuity equation can be expressed as:

$$\nabla^* \cdot \mathbf{u}^* = 0 \quad (7)$$

The dimensionless momentum conservation equation can be expressed as:

$$\rho(\mathbf{u}^* \cdot \nabla^*)\mathbf{u}^* = -\nabla^* p^* + \frac{1}{Re} \nabla^* \mathbf{u}^* - \left(1 + \frac{1}{Re}\right) \frac{1}{Da} \frac{q(1-\gamma)}{q+\gamma} \mathbf{u}^* \quad (8)$$

The energy conservation equation of the fluid region can be expressed as:

$$\rho C_p (\mathbf{u} \cdot \nabla) T = k_f \nabla^2 T \quad (9)$$

where C_p is the specific heat capacity of the fluid and k_f is the fluid thermal conductivity.

The heat transfer equation in the solid region can be expressed as:

$$0 = k_s \nabla^2 T + Q \quad (10)$$

where k_s is the thermal conductivity of the solid, and Q is the heat source term in the solid domain of the cold plate.

The transformation of the solid domain and the fluid domain in the heat transfer equation is controlled by designing the value of the variable γ , and the γ linear interpolation model is used to couple the two heat transfer equations. The general equation is thus derived as follows:

$$\gamma \rho C_p (\mathbf{u} \cdot \nabla) T = [(1-\gamma)k_s + \gamma k_f] \nabla^2 T + (1-\gamma)Q \quad (11)$$

The value of the heat source term in the solid domain is represented by the proportional relationship between the temperature change in the solid domain, and the expression is as follows:

$$Q = h(T_r - T) \quad (12)$$

where T_r is the reference temperature of the internal heat source, h is the heat coefficient of the internal heat source.

The dimensionless parameters are defined as follows:

$$T^* = \frac{T-T_c}{T_r-T_c}, Pr = \frac{\mu c_p}{k_f}, h^* = \frac{hL^2}{k_f} \quad (13)$$

where T^* indicates the inlet temperature. h^* is the dimensionless heat production coefficient, which is set to 100 in this paper based on literature.

In this study, in order to obtain a larger heat transfer area while simplifying the model, it is assumed that $k_s = k_f$, so the final dimensionless heat transfer equation can be simplified as:

$$\gamma Re Pr (\mathbf{u}^* \cdot \nabla^*) T^* = \nabla^{*2} T^* + (1-\gamma) h^* (1-T^*) \quad (14)$$

In order to control the battery temperature within a reasonable range, the liquid cooling plate must maximize the heat generated during the battery discharging process. Therefore, the heat transfer rate is taken as the objective function of the topology optimization for the liquid cooling plate. The maximum heat transfer objective function can be expressed as:

$$J = \int_{\Omega} (1-\gamma) h^* (1-T^*) d\Omega \quad (15)$$

In order to ensure the topology optimization results consistent with practical conditions, it is necessary to control the proportion of fluid domain and solid domain in the design domain, and the specific control conditions are as follows:

$$\int_{\Omega} \gamma d\Omega \leq V_{\beta} \cdot V_{\Omega} \quad (16)$$

In order to control the constant power of the inlet, the integral equation about the inlet pressure p_{in} is defined

$$\int_{\Gamma_{in}} p_{in}^* u^* d\Gamma = 1 \quad (17)$$

2.3. Calculation process

Table 1: Topology optimization design specific parameters.

Parameter	Value
Darcy number Da	10^{-4}
Penalty factor q	10^{-2}
Dimensionless heat generation h^*	100
Reynolds number Re	200
Prandtl number Pr	6.78
Dimensionless inlet temperature T_{in}^*	0
Dimensionless outlet pressure p_{out}^*	0
Volume fraction V_{β}	0.5

Topology optimization process is realized based on COMSOL, and the SNOPT optimization algorithm is adopted. The termination condition of iterations is that the objective function residual is less than 10^{-6} . The parameter values for all topology optimization designs are listed in Table 1. The specific optimization process consists of the following steps:

- Step 1: Set the constant number of topology optimization calculations, including $Re, Pr, Da, q, h^*, T_{in}^*, p_{out}^*, \beta, V_{\beta}, \gamma_{\beta}$.
- Step 2: Create the optimization model and design domain and divide the grids.
- Step 3: Set the boundary conditions, the interpolation model and objective function, and initialize the design variables.
- Step 4: Solve the governing equations for fluid flow and heat transfer.
- Step 5: Calculate the sensitivity of the objective function, and update the values of the design variable.
- Step 6: Determine whether the residuals meet the requirements; if not, return to Step 4.

Firstly, the influence of outlet quantity on topology optimization results is studied. In this study, all inlets are located in the middle of the left side of the design domain, and the width of the inlet is maintained at $2.4L$. The total outlet areas remained the same while the outlet quantity was adjusted from one to five. The outlets were evenly distributed along the cooling plate. Fig. 2 shows the topology optimized channel configurations for different outlet numbers, which were denominated as UTO-1, UTO-2, UTO-3, UTO-4 and UTO-5, respectively. With the increase of outlet number, the number of flow paths also increases, and the flow paths become more fragmented. When the number of outlets is singular, there are outlets in the middle position. When there is no outlet in the middle, a wider flow channel is formed in the center area where the fluid directly flows from the inlet to the other side and then bifurcates to the outlets along the two ends of the cold plate.

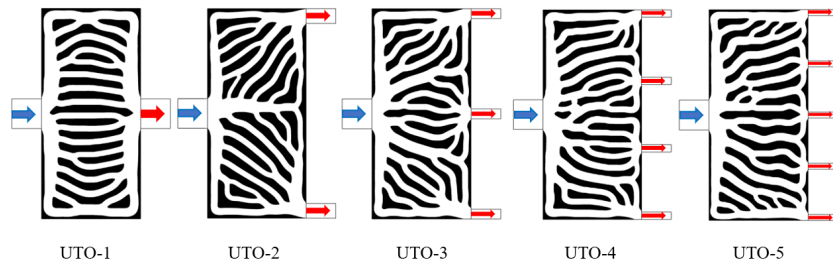


Fig. 2: Topology optimization results of different outlet numbers.

Besides, the influence of initial structures on the topology optimization results is studied. Three different initial structures with uniform distribution, straight channel and circular fins were studied. Two outlets were employed for all the three different initial structure cases. Fig. 3 shows the topology optimization results with different initial structures. The obtained topology optimized cold plate with straight channels and circular fins were denominated as SCTO and CFTO, respectively. Different initial structures could lead to different flow channel structures after topology optimization. Compared with UTO-2, the flow channel configurations of SCTO and CFTO are more curved and more fragmented.

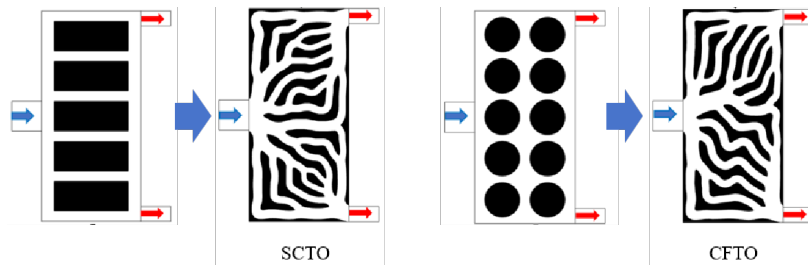


Fig. 3: Topology optimization results with different initial structures.

3. Numerical analysis

3.1 Geometric model

As shown in Fig. 4(a), the three-dimensional cold plate model is constructed by extracting the flow path boundary of the two-dimensional topology optimization results. As shown in Fig. 4(c), the length and width of the cold plate are 173mm and 85mm, respectively, the same with the battery cell dimensions, and the thickness of the cold plate is 5mm while the thickness of the flow path is 3mm. The inlet width of the flow channel is 24mm. In practical electric vehicles, at lithium

batteries are assembled to form the battery pack, as shown in Fig. 4(b), in which batteries and cold plates are alternately arranged. In this study, a symmetrical part of the battery pack is taken for investigation to simplify the calculation. As shown in the Fig. 4(d), the simulation model consists of a complete battery and two half cold plates.

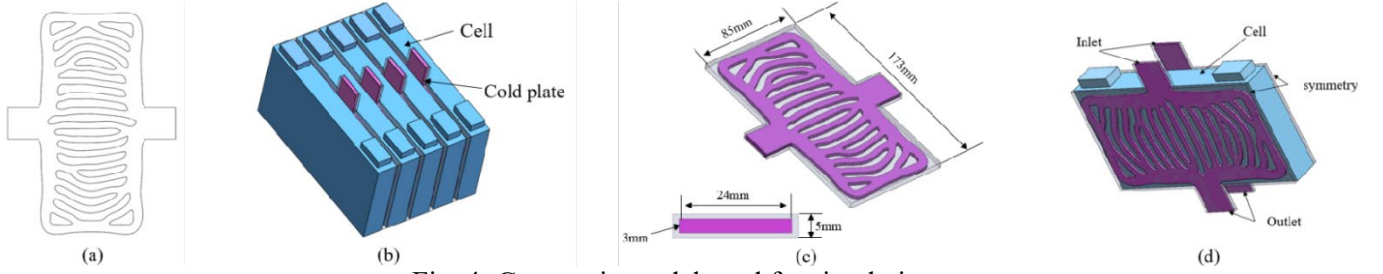


Fig. 4: Geometric model used for simulations.

Table 2: Specific physical parameters of the lithium-ion battery.

Parameter	Value
Length, Width, Height (mm)	$173 \times 85 \times 21$
Battery capacity (Ah)	22
Density ($\text{kg}\cdot\text{m}^{-3}$)	1986.2
Specific heat capacity ($\text{J}\cdot\text{kg}^{-1}\cdot\text{K}^{-1}$)	853.6
Thermal conductivity ($\text{W}\cdot\text{m}^{-1}\cdot\text{K}^{-1}$)	$19.61 \times 19.61 \times 7.78$

3.2 Governing equations for three-dimensional simulations

The continuity equation is expressed as:

$$\frac{\partial \rho_f}{\partial t} + \nabla \cdot (\rho_f \mathbf{u}_f) = 0 \quad (18)$$

where ρ_f is the coolant density and \mathbf{u}_f is the coolant flow velocity.

The momentum conservation equation is expressed as:

$$\frac{\partial (\rho_f \mathbf{u}_f)}{\partial t} + \nabla \cdot (\rho_f \mathbf{u}_f \mathbf{u}_f) = -\nabla P + \mu \nabla^2 \mathbf{u}_f \quad (19)$$

where P is the coolant pressure.

The energy equations for the fluid domain and the solid domain are:

$$\begin{cases} \rho_f C_{p,f} \frac{\partial T}{\partial t} + \nabla \cdot (\mathbf{u}_f T) = k_f \nabla^2 T, (\text{Fluid}) \\ \rho_s C_{p,s} \frac{\partial T}{\partial t} = k_s \nabla^2 T, (\text{Solid}) \end{cases} \quad (20)$$

where, $C_{p,f}$ is the specific heat capacity of coolant, $C_{p,s}$ is the specific heat capacity of solid, k_f and k_s are the thermal conductivity of the coolant and solid region, respectively, and T is the temperature.

3.3 Boundary conditions and independence tests

Water is employed as the cooling medium in this paper, and the cold plate is made of aluminum. The related thermo-physical property parameters are shown in Table 3 which remain unchanged during numerical analysis. The inlet velocity entering cold plate is 0.05m/s, and the inlet temperature equals to the ambient, i.e. 25°C. The outlet pressure is kept as 0Pa. The upper and lower surfaces of the simulation model are the cross sections of the cold plate, and the symmetric boundary conditions are applied. Natural convective heat transfer with the surrounding environment is applied for the outer walls, and the heat transfer coefficient is set as $20 \text{ W}\cdot\text{m}^{-2}\cdot\text{K}^{-1}$ after validation with the experimental data.

Table 3: Liquid cooling plate and coolant physical parameters.

Properties	C_p ($\text{J}\cdot\text{kg}^{-1}\cdot\text{K}^{-1}$)	k ($\text{W}\cdot\text{m}^{-1}\cdot\text{K}^{-1}$)	ρ ($\text{kg}\cdot\text{m}^{-3}$)	μ (Pa·s)
Liquid cooling plate (Aluminum)	903	237	2702	-
Coolant (Water)	4186.72	0.62	997.56	0.001003

In order to balance the accuracy of the simulation results and the computational cost, the effects of grid numbers and time steps on maximum temperature of the lithium-ion battery and flow channel pressure drop were compared to realize the independence check of grid and time step. According to the results in Fig. 5, the grid number of 962,135 and the time step of 1s were finally selected.

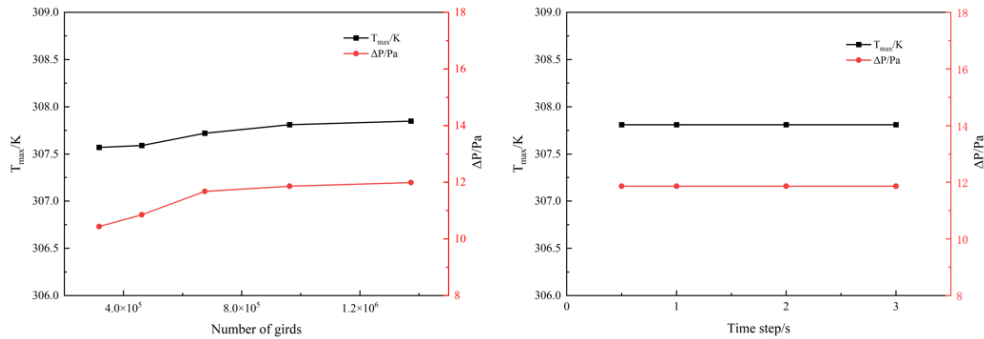


Fig. 5: Grid and time step independence verification.

4. Result analysis

4.1 Impact of outlet quantity

Fig. 6 shows the maximum temperature, average temperature and pressure drop of the cases with different outlet numbers at the inlet flow velocity of 0.05m/s. As can be seen from Fig. 8(a), when the number of outlets is one, it presents the largest maximum and average temperatures. When the number of outlets is two, the smallest maximum and average temperatures are achieved, which decrease by 2.48K (25.7%) and 1.07K (15.6%), respectively, compared with that of UTO-1 case. When the number of outlets increases, the change trend of the maximum and average temperatures is the same. They reach relatively stable with the increase of the number of outlets. It also can be found that, the temperatures for UTO-2 and UTO-4 cases are relatively low, and they are relatively high when the number of outlets is odd. The reason for this situation may be that there are intermediate outlets when the number of outlets is one, three and five. In this case, a lot of coolant enters from the middle and then directly flows toward the outlet at the middle, thus lowering the cooling efficiency. It can be seen from Fig. 6(b) that when the outlet quantity is three, the pressure drop is the smallest, which is 0.73Pa lower than that when the outlet quantity is one. It is also found that under the same power consumption, the maximum temperature is the smallest when the number of outlets is 2.

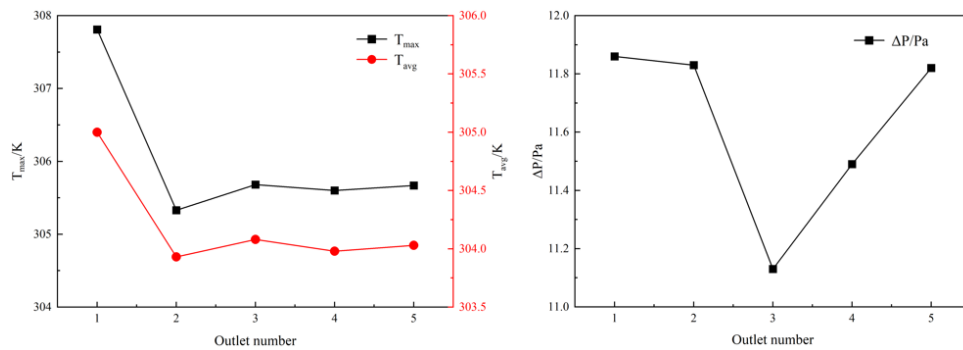


Fig. 6: Maximum temperatures, average temperatures and pressure drops for different outlet numbers.

Fig. 7 shows the temperature distributions at the middle plane of the battery and the velocity contour plots at the middle plane of the cold plate. It can be seen that the flow rate in the central region of UTO-1 case is high, resulting in a large amount of coolant flowing out of the cold plate only in the central region, and only a small amount of coolant flow toward the sides of the cold plate, resulting in uneven temperature distribution and hot spots at the two ends of the battery. By placing the outlets at the ends of the cold plate after increasing the outlet number, the problem of uneven temperature distribution can be effectively improved. It can be seen from the figure that after increasing the outlet, the flow velocity within the branch channels away from the central region is increased, and the coolant flows more evenly in the cold plate. Since the total

volume of exports remains the same, as the number of outlets increases, the width of the outlets decreases, which causes the growth of the outlet velocity.

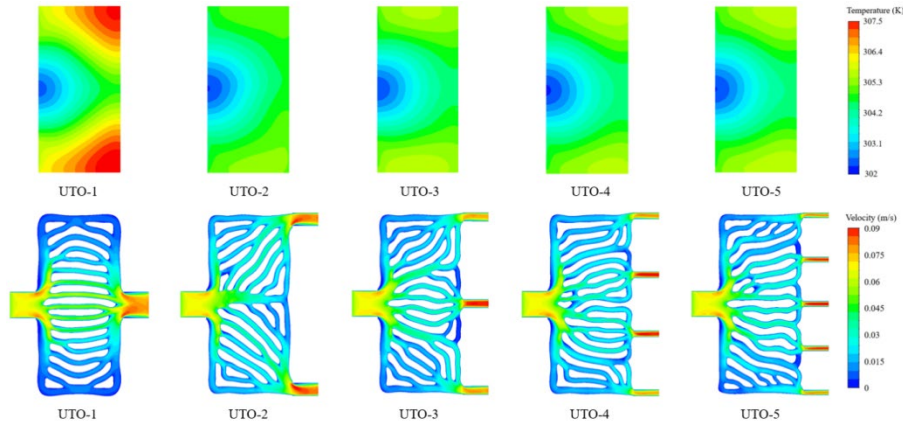


Fig. 7: Temperature cloud image and velocity cloud image with different number of outlets.

4.2 Impact of initial structure

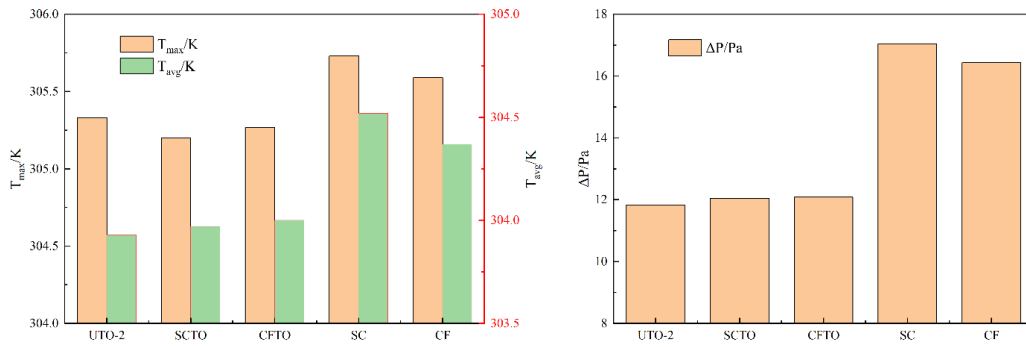


Fig. 8: Maximum temperature, average temperature and pressure drop for cases with different initial structures.

Fig. 8 shows the maximum temperature of the battery and average pressure drop of the cold plate with different initial structures after topology optimization at the inlet velocity of 0.05m/s. It can be seen that all the topology optimized cold plates perform better than the initial cold plates of SC and CF in terms of both the temperature and pressure drop. The SCTO cold plate has the lowest battery temperature, which is 0.51 ° C (7%) lower than the SC cold plate. As for the average temperature, there is little difference between the three kinds of topology optimization cold plates. UTO-2 cold plate presents the lowest pressure drop, 5.22Pa (30.6%) lower than SC cold plate.

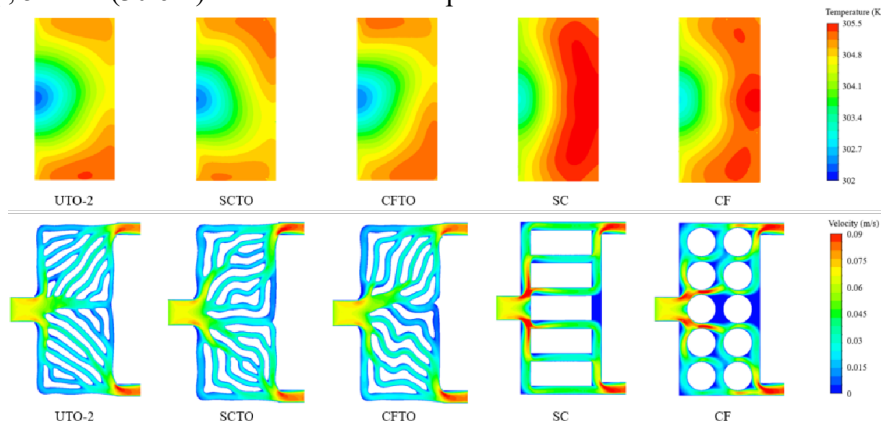


Fig. 9: Temperature and velocity contour plots for cases with different initial structures.

Fig. 9 shows the temperature distribution on the middle plane of the battery and the velocity distribution on the middle plane of the cold plate. It can be seen that these topology optimized cold plates effectively eliminate the occurrence of high temperature regions of the battery, and there are a large portion of high temperature regions in the middle plane of the SC cold plate and the CF cold plate cases. As can be seen from the velocity distribution diagram, the velocity distribution in the topology optimized cold plate is relatively uniform, and the coolant can be evenly distributed in the cold plate, thus avoiding the generation of high temperature areas of the battery. In the SC and CF cold plate, a large number of refrigerant flows to both sides due to the existence of the middle partition, and there are flow dead zones in the central area. The heat generated by the battery cannot be transferred away effectively, resulting in the occurrence of high temperature areas.

5. Conclusion

The topology optimization design of liquid cold plate for battery thermal management is studied. The influences of outlet layouts and initial structures on the topology optimization results are examined. The main findings are as follows:

(1) Increasing the number of outlets can effectively improve the heat exchange efficiency of topology optimized cold plates. Optimal performance is attained when the outlet count is 2 under the conditions of this study, resulting in maximum and average temperature reductions of 2.48K (25.7%) and 1.07K (15.6%), respectively, relative to a singular outlet.

(2) Disparate initial structures yield varied topology optimization results. Notably, post-optimization design based on the straight channel exhibits the most subdued battery temperature, registering a further decrease of 0.51°C (7%) compared to its unoptimized counterpart. Concurrently, the uniformly distributed topologically optimized cold plate manifests the least pressure drop, plummeting by 5.22Pa (30.6%) in contrast to the straight channel cold plate.

Acknowledgements

This research was financially supported by National Key Research and Development Program of China (Grant No. 2023YFB4301700), Innovation Team Project of the Chinese Ministry of Education of China (8091B042204), National Natural Science Foundation of China (Grant No. 52306070), Natural Science Foundation of Liaoning Province (Grant No. 2023010455-JH3/101).

References

- [1] J. Xu, Z. Guo, Z. Xu, X. Zhou, and X. Mei, "A systematic review and comparison of liquid-based cooling system for lithium-ion batteries," *eTransportation*, vol. 17, p. 100242, Jul. 2023,
- [2] X. Feng, M. Ouyang, X. Liu, L. Lu, Y. Xia, and X. He, "Thermal runaway mechanism of lithium ion battery for electric vehicles: A review," *Energy Storage Materials*, vol. 10, pp. 246–267, Jan. 2018,
- [3] W. Mei, H. Chen, J. Sun, and Q. Wang, "Numerical study on tab dimension optimization of lithium-ion battery from the thermal safety perspective," *Applied Thermal Engineering*, vol. 142, pp. 148–165, Sep. 2018,
- [4] H. Liu, Z. Wei, W. He, and J. Zhao, "Thermal issues about Li-ion batteries and recent progress in battery thermal management systems: A review," *Energy Conversion and Management*, vol. 150, pp. 304–330, Oct. 2017,
- [5] H. Liu, H. Li, Y. Shi, and Y. Ji, "Performance Evaluation of a Novel Cold Plate with Double-Layer Interdigitated Flow Channels for Battery Thermal Management," *Heat Transfer Engineering*, vol. 0, no. 0, pp. 1–15,
- [6] W. Li, M. Xiao, X. Peng, A. Garg, and L. Gao, "A surrogate thermal modeling and parametric optimization of battery pack with air cooling for EVs," *Applied Thermal Engineering*, vol. 147, pp. 90–100, Jan. 2019,
- [7] S. Cai, X. Zhang, and J. Ji, "Recent advances in phase change materials-based battery thermal management systems for electric vehicles," *Journal of Energy Storage*, vol. 72, p. 108750, Nov. 2023,
- [8] H. Liu, S. Ahmad, Y. Shi, and J. Zhao, "A parametric study of a hybrid battery thermal management system that couples PCM/copper foam composite with helical liquid channel cooling," *Energy*, vol. 231, p. 120869, Sep. 2021,
- [9] M. Suresh Patil, J.-H. Seo, and M.-Y. Lee, "A novel dielectric fluid immersion cooling technology for Li-ion battery thermal management," *Energy Conversion and Management*, vol. 229, p. 113715, Feb. 2021,
- [10] H. Liu, X. Gao, J. Zhao, M. Yu, D. Niu, and Y. Ji, "Liquid-based battery thermal management system performance improvement with intersected serpentine channels," *Renewable Energy*, vol. 199, pp. 640–652, Nov. 2022,
- [11] H. Li, X. Ding, D. Jing, M. Xiong, and F. Meng, "Experimental and numerical investigation of liquid-cooled heat sinks designed by topology optimization," *International Journal of Thermal Sciences*, vol. 146, p. 106065, Dec. 2019,